ELSEVIER

Contents lists available at ScienceDirect

Thermochimica Acta

journal homepage: www.elsevier.com/locate/tca



Short communication

The effect of supercooling of the melt on the semicrystalline morphology of PA 66



Anne M. Gohn^{a,b}, Alicyn M. Rhoades^{a,*}, Nichole Wonderling^b, Tim Tighe^b, René Androsch^c

- ^a School of Engineering, Penn State Behrend, 4701 College Drive, Erie, PA 16563, United States
- b Materials Characterization Lab, Penn State, N-050 Millennium Science Complex, Pollock Road, University Park, PA 16802, United States
- ^c Interdisciplinary Center for Transfer-oriented Research, Martin Luther University Halle-Wittenberg, 06009 Halle/Saale, Germany

ARTICLE INFO

Keywords: Polyamide 66 Crystallization Crystal nucleation Crystal morphology Crystal polymorphism Fast scanning chip calorimetry

ABSTRACT

Fast scanning chip calorimetry (FSC) was used to prepare isothermally crystallized samples of polyamide 66 (PA 66) in a wide range of temperatures between 70 and 230 °C for subsequent analysis of the semicrystalline morphology by X-ray diffraction, polarized-light optical microscopy and atomic force microscopy. At high crystallization temperatures stable triclinic α -crystals of lamellar shape, organized within a spherulitic superstructure are formed. At low crystallization temperatures, in contrast, the less stable pseudohexagonal γ -crystal structure/mesophase develops. The mesophase of PA 66, which forms at temperatures close to the glass transition, is of grainy, non-lamellar habit, and not organized within spherulites. The formation of such qualitatively different semicrystalline morphologies of PA 66 is suggested to be caused by different densities of crystal nucleation, supported by observation of a bimodal temperature-dependence of the crystallization rate. The experimental findings reported in this work are important to allow tailoring of the microstructure of PA 66 by variation of the conditions of processing as well as contribute to the ongoing research about crystal nucleation in polymers.

1. Introduction

Polyamide 66 (PA 66) is an important engineering thermoplastic material used in a variety of markets ranging from automotive, sporting goods, aerospace, and fiber industry [1–3]. It is an attractive polymer for many applications because it is a tough, strong, durable material with excellent chemical and temperature resistance, and good wear properties [4]. As in case of all polymeric materials, many of these properties depend on the semicrystalline structure [5–8], and therefore much effort has been undertaken exploring the relation between the conditions of solidification, the resulting microstructure and the properties of this material [9–11]. Focus of the present study is the evaluation of microstructure/semicrystalline morphology of PA 66 forming at different condition of solidification the supercooled melt, with emphasis placed on the analysis of the crystal polymorphism, the formation of a higher-order superstructure, and the crystal morphology.

PA 66 forms multiple/different crystal polymorphs whose development is dependent on the conditions of crystallization [12–18]. With regard to crystallization of the quiescent melt, there has been reported formation of either $\alpha\text{-}crystals$ or $\gamma\text{-}mesophase.$ In the more stable $\alpha\text{-}crystals$, which develop on slow cooling of the quiescent melt or at

rather high temperature, the molecules arrange in a triclinic unit cell. The methylene units adopt a planar zigzag conformation and the hydrogen bonds, which connect the amide groups between neighbored chain segments, show a sheet-like planar arrangement [12]. On heating, the α -form transforms at the Brill transition temperature into its high-temperature α '-modification with a pseudohexagonal unit cell [19,20]. The transition is reversible, that is, the α '-phase converts on cooling into the α -phase, and cannot be observed at room temperature. In the pseudohexagonal γ -mesophase, a non-planar arrangement of hydrogen bonds is suggested [13]. It develops upon quenching of the melt [13], and is only metastable at the temperature of formation and lower temperatures, as on heating the γ -mesophase converts irreversibly into α'/α -crystals [21].

The transition of the melt into α/α' -crystals on slow cooling/high temperature is connected with the formation of lamellae and spherulites [22–25]. Details of the morphology and superstructure of the γ -mesophase of PA 66, and their exact conditions of formation, however, are completely unknown to date. In case of PA 6 and PA 11, which exhibit a similar crystal/mesophase polymorphism controlled by the cooling rate/supercooling as PA 66 [26–30], the mesophase is of non-lamellar habit and not spatially organized in a higher-order

E-mail address: amh234@psu.edu (A.M. Rhoades).

^{*} Corresponding author.

A.M. Gohn et al. Thermochimica Acta 655 (2017) 313–318

superstructure [31-33]. In the present study, we attempt proving that PA 66 shows a similar dependence of the semicrystalline morphology on the condition of melt-crystallization as observed before for PA 6 and PA 11. It is, however, worthwhile noting that analysis of the crystallization behavior at high supercooling of the melt, at temperatures close to the glass transition, is complicated since crystallization often begins before the system reaches the target analysis temperature. Outpacing these kinetics requires application of high cooling rates, much higher than in conventional differential scanning calorimetry (DSC), which assures absence of crystallization at low supercooling of the melt. With the use of fast scanning chip calorimetry (FSC) it is possible to transfer the equilibrium melt to any temperature, allowing analysis of the isothermal crystallization kinetics starting with a supercooled melt free of crystals [34,35]. In addition, samples subjected to well-defined crystallization-histories in an FSC can then be used for structural analyses including atomic force microscopy (AFM) [31], polarized-light optical microscopy (POM) [36], or X-ray diffraction (XRD) [37,38]. In the present study, that approach is applied for PA 66 in order to provide for this important polymer structure information after solidification of the supercooled melt at temperatures close to the glass transition temperature. It was discovered that two maxima in crystallization rate were observed around 160 and 115 °C. The high temperature crystallization was found to produce the stable triclinic α -crystal, whereas the low temperature crystallization produced the pseudohexagonal y-mesophase. Around 110-120 °C there was a transition from the spherulitic structure to non-spherulitic structure at low and high supercooling, respectively. These information can then be used to intentionally produce in an efficient and predictable way different semicrystalline morphologies, by modification of processing routes, with the final aim of tailoring properties. As prominent examples for demonstration of structure-property relations, it was shown early for the specific case of PA 66, that mechanical properties are largely controlled by the size of spherulites [39] or, investigated on PA 6, that Young's modulus and the hardness of the α -crystals are about twice than that of the γ -mesophase

2. Experimental

2.1. Material

The material used in this study was Zytel 101 from DuPont (USA). It is an un-lubricated and unmodified general-purpose molding-viscosity PA 66 grade [41], selected in this study to ensure that no additives are present which would affect the crystallization process. The number-average molar mass of this polymer is around 17–18 kDa [42]. The material was delivered in form of dry pellets, which were cut using a rotary microtome equipped with a tungsten carbide blade to obtain thin sections. Their thickness and lateral dimension, with the latter adjusted using a scalpel and a stereomicroscope, were 12 and about 50 μm , respectively, for FSC analysis of the crystallization kinetics, and 20 and about 300 μm for FSC preparation of samples for AFM, POM and XRD.

2.2. Instrumentation

2.2.1. Fast scanning chip calorimetry (FSC)

FSC analysis allowed for thermal preconditioning of the samples prior to XRD, POM and AFM analyses. Furthermore, FSC was used to obtain information about the temperature-dependence of the isothermal crystallization rate of the specific PA 66 grade employed in this study. Measurements of the crystallization kinetics were done using two Flash DSC 1 devices from Mettler-Toledo. Both instruments were operated in conjunction with a Huber TC100 intracooler, and the sensor/sample environment was purged with nitrogen gas using a flow rate of 35 mL/min to prevent sample degradation and icing of the equipment. According to the recommendation of the instrument provider, the FSC sensors were conditioned and temperature-corrected before loading of a

sample. When using the FSC for thermal preconditioning of samples, in case of XRD and POM analyses, all measurements were performed on a single sample. In other words, the sample attached to the sensor was removed from the FSC after a specific thermal treatment, analyzed regarding its structure, and then re-inserted into the FSC to impose the next thermal history. Only in case of the AFM analyses, sensors needed to be destroyed for optimum sample preparation.

2.2.2. X-ray diffraction (XRD)

XRD measurements of the preconditioned FSC samples were performed using a Rigaku DMAX-Rapid II diffractometer equipped with a Cu X-ray tube and a graphite monochromator. Analyses were done in transmission mode, and the scattered X-rays were recorded using a curved image plate coated with photo-stimulable phosphor (BaF (Br,I):Eu 2)The beam diameter and exposure time were 300 μm and 600 s, respectively. The 2D XRD patterns were azimuthally integrated to yield the intensity distribution as a function of the scattering angle 20, followed by subtraction of an XRD curve obtained on an empty FSC chip.

2.2.3. Polarized-light optical microscopy (POM)

POM images of FSC samples subjected to a specific crystallization history were obtained using a Leica DMRX microscope operated in reflection mode and with the sample placed between crossed polarizers. Images were captured using a Motic 2300 CCD camera and imaging software.

2.2.4. Atomic force microscopy (AFM)

AFM measurements were performed using a Bruker Dimension Icon. Samples were conditioned isothermally on the FSC chip before rapid cooling to room temperature. The sensor/membrane was then fractured away from the ceramic frame in order to transfer the sample to a stainless steel specimen disc using double-sided adhesive tape. PeakForce tapping imaging mode was used with a ScanAsyst Air Probe (0.4 N/m spring constant). Image analysis was done using Nanoscope Analysis software.

3. Results and discussion

Fig. 1 shows FSC crystallization curves, heat-flow rate as a function of time, recorded at temperatures between 220 °C (front curve) and 75 °C (back curve), after the sample was cooled from 300 °C at a rate of 2000 K/s to the crystallization temperature. Inspection of the peak-time of crystallization reveals, as expected, a bimodal temperature-dependence of the crystallization rate, similar as has been observed recently on a different PA 66 grade [44]. Upon investigating isothermal crystallization temperatures, the peak-time of crystallization decreases due

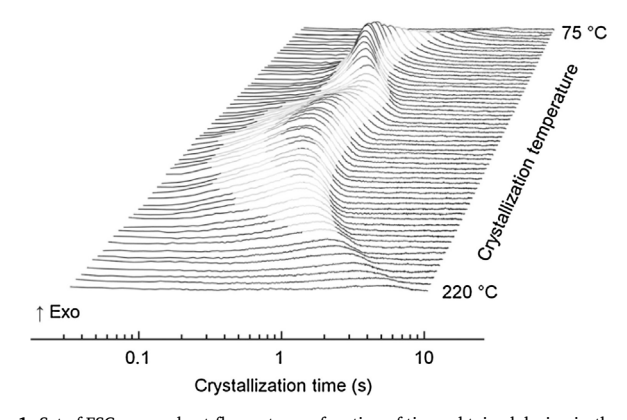


Fig. 1. Set of FSC curves, heat-flow rate as a function of time, obtained during isothermal crystallization of PA 66 (Zytel 101) at temperatures between 220 $^{\circ}\text{C}$ (front curve) and 75 $^{\circ}\text{C}$ (back curve). The temperature-difference between two neighbored curves is 2.5 K. Exothermic heat flow is upward directed.

A.M. Gohn et al. Thermochimica Acta 655 (2017) 313–318

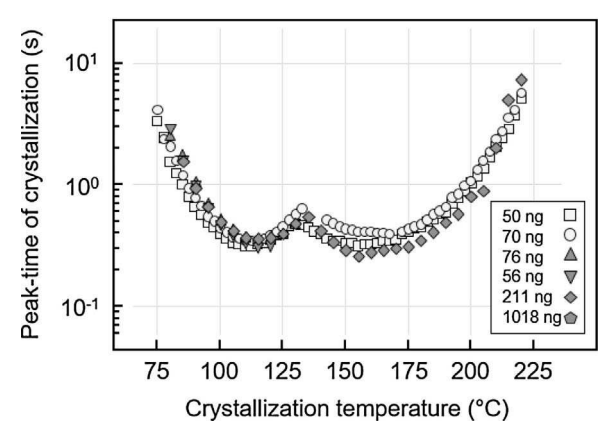


Fig. 2. Peak-time of isothermal crystallization of PA 66 (Zytel 101) as a function of the crystallization temperature. Dark- and light-gray symbols refer to measurements performed using different instruments, while the different symbols represent the use of samples of different mass between about 50 and 1000 ng.

to the increasing thermodynamic driving force for the phase transition until a maximum rate of crystallization is observed at 160 °C. Further reduction of the temperature causes the rate to slightly increases due to constraints related to decreasing mobility of molecular segments. At increasingly lower temperature, however, there is observed a second peak-time minimum at 115 °C, which for many polymers [34–36] has been associated with a drastic increase of the nucleation rate when homogeneous nucleation becomes dominant at temperatures close to the glass transition.

Quantitative peak-time data are shown in Fig. 2 as a function of the crystallization temperature, with the dark and light gray symbols referring to measurements, which were performed using two different FSC instruments, for the sake of checking the reproducibility. Crystallization-rate maxima, presumably related to heterogeneous and homogeneous nucleation are observed at about 160 and 115 °C, respectively, with the corresponding characteristic crystallization times being around 0.3 s in both cases. The transition from pre-dominant heterogeneous nucleation at high temperature, to pre-dominant homogeneous nucleation at low temperature occurs at around 130 °C. The isothermal crystallization time of PA 66 has previously been studied by FSC analysis [44], and the analysis here confirms the findings. While for PA 6, PA 11, iPP, or PBT, information about the semicrystalline morphology formed on crystallization at low temperatures and about the change of the nucleation mechanism on variation of the crystallization temperature are available [31-37], for PA 66 such data are still lacking. Therefore, in order to assess the effect of the crystallization temperature on structure formation, assuring absence of crystallization on the approach of the crystallization temperature, FSC with its high cooling capacity has been used to prepare samples, which then are analyzed by XRD, POM and AFM, shown below.

Fig. 3 is a plot of XRD curves of samples of PA 66 which were isothermally crystallized for 200 s in the FSC after cooling the melt from 300 °C to different crystallization temperatures between 70 and 230 °C at a rate of 800 K/s, as is indicated to the right of the various curves. Note that compared to the FSC measurement of characteristic crystallization times (Figs. 1 and 2) the cooling rate was lower (800 instead of 2000 K/s) in order to account for the higher sample mass which is advantageous for X-ray analyses since increasing the S/N-ratio. Furthermore, a crystallization time of 200 s is considered sufficient to complete primary crystallization according to the crystallization peaktimes data shown in Fig. 2.

The data of Fig. 3 reveal the expectation that on crystallization at high temperature there is formation of α -structure, which is indicated with the detection of the characteristic diffraction peaks labeled $\alpha 1$ and $\alpha 2$ at 20.3 and 23.7 deg 20, associated to the (100) and (010)/(110) lattice planes of the triclinic unit cell [12,45]. With decreasing

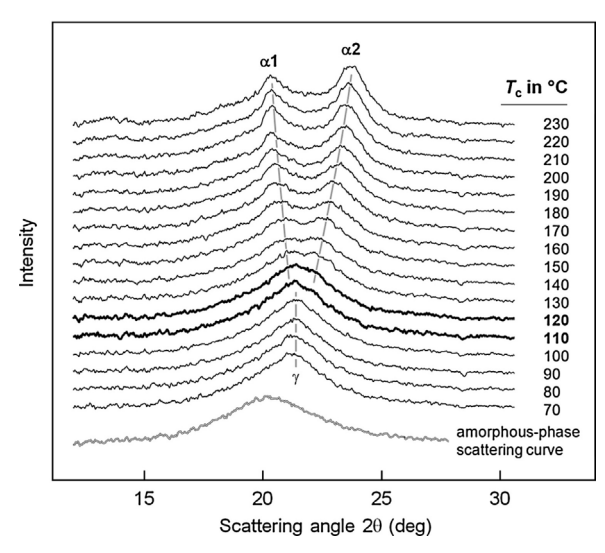


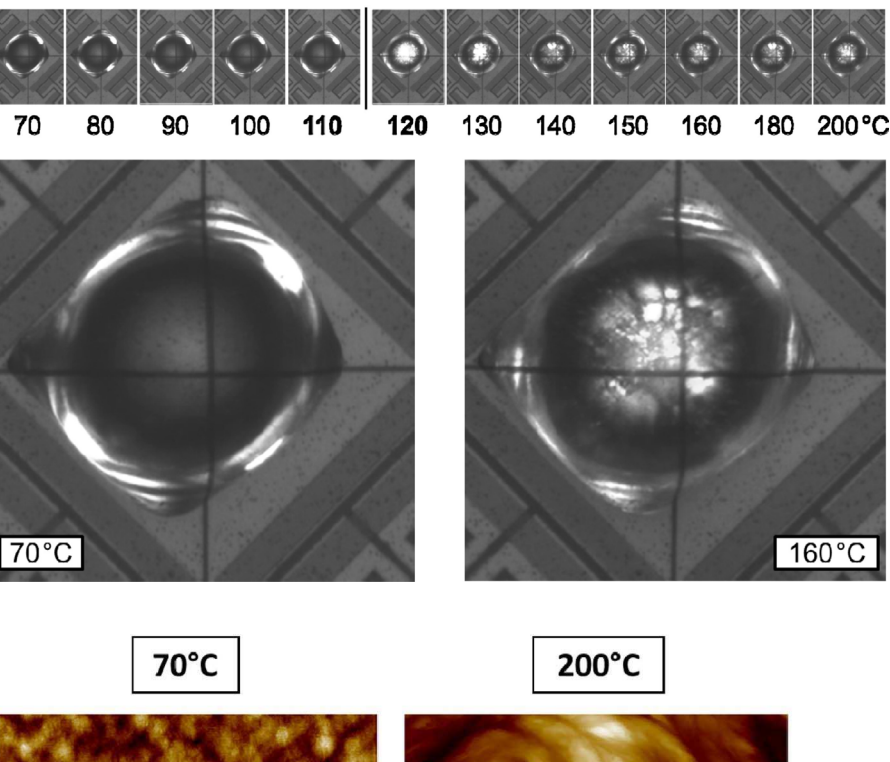
Fig. 3. XRD patterns of amorphous PA 66 (Zytel 101) (bottom curve) and PA 66 which was isothermally crystallized at temperatures (T_c) between 70 and 230 °C, as is indicated at the right-hand side of the curves.

crystallization temperature, the distance between the $\alpha 1$ and $\alpha 2$ diffraction peaks decreases, indicating loss of crystal perfection [46], that is, loss of perfect, sheet-like alignment of hydrogen bonds between neighbored chain segments. The change of the dimensions of the unit cell in cross-chain direction seems gradual, and in samples crystallized at temperatures lower than about 130 °C the $\alpha 1$ and $\alpha 2$ peaks are strongly overlapping and difficult to distinguish. At temperatures lower than 120 °C only the 100 peak of the pseudohexagonal γ -mesophase of PA 66 is detected at about 21.4 deg 29 [13]. The lowermost XRD scan in Fig. 3 was obtained on a sample continuously cooled at a rate of 800 K/s to room temperature, which led to suppression of crystallization. As such, it reveals scattering of the amorphous phase only and confirms with the position of the maximum of the halo at about 20.2 deg 20 that the peak in the XRD scans of samples crystallized between 70 and 110 °C indeed is due to formation of an ordered phase.

In order to obtain information about the superstructure formed by the ordered phase within in the amorphous matrix, samples isothermally crystallized in the FSC have been imaged by polarized-light optical microscopy in reflection mode. Fig. 4 provides with the images in the top row an overview about the effect of the crystallization temperature on the POM-structure, revealing that crystallization between 120 and 200 °C leads to a bright appearance of the sample due to distinct birefringence; even spherulites of different size can be detected. It appears that the nuclei density increases with decreasing temperature in particular in samples crystallized below 130 °C as then individual spherulites cannot be identified anymore, though the sample is still appearing bright. Only if the crystallization temperature is lower than 120 °C then the samples appear featureless and apparently do not show birefringence. The two enlarged photographs below the top row of images show the typical microstructure of samples crystallized at high (left image) and low (right image) supercooling of the melt, resembling earlier studies of the POM-structure of both, samples isothermally crystallized at different temperatures in an FSC [37], or film samples crystallized at largely different supercooling [32,47-49]. In none of the investigated samples of iPP, PA 6, PA 11, or PBT, crystallization at high supercooling is connected with the formation of spherulites, as the nuclei density is too high for growth of micrometer-size birefringent

Information about the nanometer-scale structure of samples crystallized at largely different supercooling, finally, was obtained by AFM. As in case of XRD and POM analyses, samples were crystallized in the FSC in order to ensure isothermal crystallization conditions. After the isothermal crystallization step, the samples were rapidly cooled to room

Thermochimica Acta 655 (2017) 313–318



A.M. Gohn et al.

Fig. 4. POM micrographs of samples of PA 66 (Zytel 101) isothermally melt-crystallized at the indicated temperatures (top row). The large images were obtained on samples crystallized at 70 (left) and 160 °C (right).

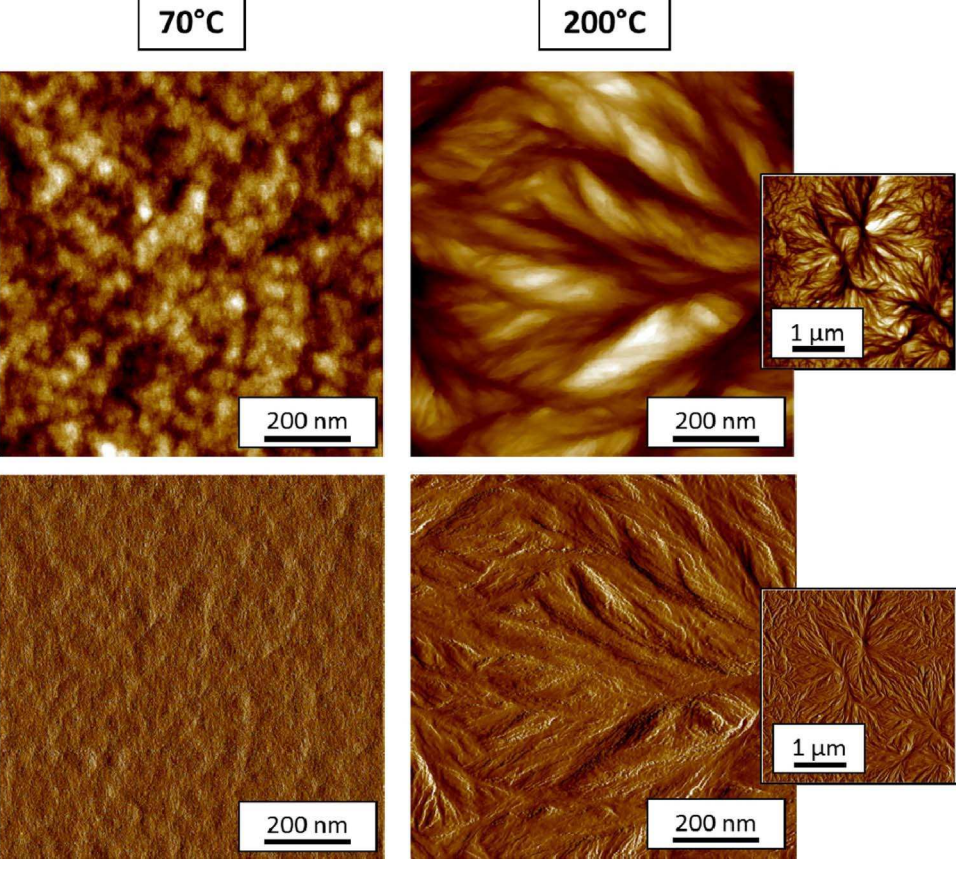


Fig. 5. AFM images of samples of PA 66 (Zytel 101) isothermally melt-crystallized at 70 °C (left) and 200 °C (right). Top row images show height mode scans, and bottom row images show error mode scans. An insert of the 200 °C sample at lower magnification is included to display the spherulitic structure formed at low supercooling.

temperature, and then the FSC membrane together with the sample was prepared on AFM steel mounting disks using adhesive pads. The images in Fig. 5 are AFM height- and error-mode contrast images of the surface of PA 66 samples, which were crystallized at 70 and 200 °C. The figures in the left column display samples crystallized at 70 °C, and the figures in the right column display samples crystallized at 200 °C. The top row images were formed using height mode imaging in the AFM, and the bottom row images show error mode imaging. These samples were prepared multiple times in order to confirm consistency in the microstructure. The sample crystallized at 70 °C required additional repeated

imaging attempts due to surface artefacts obscuring the surface structure. Visual inspection of the images reveals qualitatively different nanometer-scale structures of PA 66 formed on crystallization at low and high supercooling. The right images shows several spherulites with a diameter of few micrometers, to be recognized by their centers of symmetry. The striations along the radius point to formation of laterally extended lamellae, which is related to the rather low nucleation density and available volume for growth. Crystallization at high supercooling, in contrast, is not connected with spherulitic growth of lamellae as the left image in Fig. 5 shows with the bright spots particle-like domains

A.M. Gohn et al. Thermochimica Acta 655 (2017) 313–318

with a size of perhaps 10–20 nm. The obviously spatially non-organized/independent growth of these domains supports the notion that each of these domains was a former crystal nucleus, and that the nucleation density on crystallization at high supercooling of the melt is several orders of magnitude higher than on crystallization at low melt-supercooling. From the XRD data of Fig. 3 it is concluded that these domains represent the γ -mesophase of PA 66, while the spherulitically grown lamellae in the right image represent/possess α -structure.

4. Conclusions

Information about the semicrystalline morphology of PA 66 isothermally forming at high supercooling of the melt is not available to date. This lack of knowledge is caused by difficulties in transferring the relaxed-melt state to low temperatures without crystallization during the cooling step/approach of the crystallization temperature; in prior work it has been quantified for PA 66 that cooling at rates of several hundred K/s is required to assure absence of crystallization during cooling [44]. In order to perform well-defined isothermal crystallization experiments in a wide range of temperatures between 70 and 230 °C, FSC with its high cooling capacity has been employed for both analysis of crystallization rates as well as preparation of samples for subsequent analysis of the semicrystalline morphology by XRD, POM, and AFM. The crystallization rate of PA 66 shows a bimodal distribution versus temperature, with two distinct maxima observed at around 160 and 115 °C. Structure analyses revealed that at relatively high crystallization temperatures stable triclinic α -crystals form, which are laterally extended, and arranged in a spherulitic superstructure. In contrast, at low crystallization temperatures, around the low-temperature crystallization-rate maximum, the less stable pseudohexagonal γ-crystal mesophase develops, which is of non-lamellar, particle-like shape and not growing spherulitically. The independently grown mesophase domains suggest that the nucleation density at high supercooling of the melt is distinctly higher than at low supercooling of the melt; note that the distance between two neighbored crystal nuclei on crystallization at low and high supercooling of the melt is of the order of magnitude of several micrometer and few ten nanometer, respectively. In particular POM analysis of FSC samples crystallized at different temperatures leads to the suggestion that the transition from the spherulitic to the non-spherulitic semicrystalline morphology, developing at low and high supercooling of the melt, respectively, occurs in a rather narrow temperature range around 110-120 °C but not gradual. This points to a qualitative change of the mechanism of crystal nucleation, namely from heterogeneous nucleation at high temperature to homogeneous nucleation at low temperature, and explains the occurrence of two distinctly separated crystallization-rate maxima at different temperatures. The experimental observations reported in this study we consider important to allow tailoring of the microstructure and therefore of properties of PA 66 by variation of the processing conditions.

Acknowledgment

This work was supported by the National Science Foundation under grant no. 1653629.

References

- [1] M.I. Kohan, Nylon Plastics Handbook, Hanser/Gardner Publications, Inc., Cincinatti, OH, 1995.
- [2] L.B.R. Bottenbruch, Polyamides as Engineering Thermoplastic Materials, Rapra Technology Limited, 2000.
- [3] T.A. Osswald, G. Menges, Materials Science of Polymers for Engineers, Hanser/ Gerdner Publications, Inc., Cincinatti, OH, 2003.
- [4] J.A. Brydson, Plastics Materials, Butterworth-Heinemann Ltd., Oxford, 1995.
- [5] H. Janeschitz-Kriegl, Crystallization Modalitites in Polymer Melt Processing, Springer Wein, New York, 2010.
- [6] E. Piorkowski, G.C. Rutledge, Handbook of Polymer Crystallization, Wiley, Hoboken, NJ, 2013.

[7] D. Drummer, S. Meister, Correlation of processing, inner structure, and part properties of injection moulded thin-wall parts on example of polyamide 66, Int. J. Polym. Sci. (2014) 1–8.

- [8] S. Meister, D. Drummer, Influence of manufacturing conditions on measurement of mechanical material properties on thermoplastic micro tensile bars, Polym. Test. 32 (2013) 432–437.
- [9] H.W. Starkweather, G.E. Moore, J.E. Hansen, T.M. Roder, R.E. Brooks, Effect of crystallinity on the properties of nylons, Poly. Chem. 18 (1956) 189–204.
- [10] H.W. Starkweather, R.E. Brooks, Effect of spherulites on the mechanical properties of nylon 66, Appl. Polym. Sci. (1959) 236–239.
- [11] D. Drummer, A. Seefried, S. Meister, Characterization of material stiffness on injection moulded microspecimens using different test methods, Adv. Mater. Sci. Eng. (2014) 1–8
- [12] C.W. Bunn, E.V. Garner, The crystal structures of two polyamides (nylons), Proc. R. Soc. Lond. (1947) 39–68.
- [13] G.F. Schmidt, H.A. Stuart, Gitterstrukturen mit räumlichen Wasserstoffbückensystemen und Gitterumwandlungen bei Polyamiden, Zeitschr. Naturforsch. (A) 13 (1958) 222–225.
- [14] A. Keller, A. Maradudin, Diffraction of x-rays by fibres consisting of small crystals: application of theory to polyamides, J. Phys. Chem. Solids 2 (1957) 301–311.
- [15] M.L. Colclough, R. Baker, Polymorphism in nylon 66, J. Mater. Sci. 13 (1978) 2531–2540.
- [16] H.W. Starkweather, G.A. Jones, Crystalline transitions in powders of nylon 66 crystallized from solution, J. Polym. Sci. Polym. Phys. 19 (1981) 467–477.
- [17] S. Dasgupta, W.B. Hammond, W.A. Goddard III, Crystal structures and properties of nylon polymers from theory, J. Am. Chem. Soc. 118 (1996) 12291–12301.
- [18] N.A. Jones, E.D.T. Atkins, M.J. Hill, Investigation of solution-grown, chain-folded lamellar crystals of the even-even nylons: 6 6 8 6, 8 8, 10 6, 10 8, 10 10, 12 6, 12 8, 12 10, and 12 12, J. Polym. Sci. Polym. Phys. 38 (2000) 1209–1221.
- [19] R. Brill, Über das Verhalten von Polyamiden beim Erhitzen, J. Prakt. Chem. 161 (1942) 49–64.
- [20] R. Brill, Beziehungen zwischen Wasserstoffbindung und einigen Eigenschaften von Polyamiden, Makromol. Chemie 18 (1956) 294–309.
- [21] R. Androsch, M. Stolp, H.-J. Radusch, Crystallization of amorphous polyamides from the glassy state, Acta Polym. 47 (1996) 99–104.
- [22] F. Rybnikář, P.H. Geil, Melting and recrystallization of PA-6/PA-66 blends, J. Appl. Polym. Sci. 49 (1993) 1175–1188.
- [23] F. Khoury, The formation of negatively birefringent spherulites in polyhexamethylene adipamide (nylon 66), J. Polym. Sci. 33 (1958) 389–403.
- [24] J.H. Magill, Formation of spherulites in polyamide melts: part III. Even-even polyamides, J. Polym. Sci. Part A 4 (2) (1966) 243–265.
- [25] B.B. Burnett, W.F. McDevit, Kinetics of spherulite growth in high polymers, J. Appl. Phys. 28 (1957) 1101–1105.
- [26] L.G. Roldan, H.S. Kaufman, Crystallization of nylon 6, J. Polym. Sci. Polym. Lett. 1 (1963) 603–608.
- [27] A. Ziabicki, Über die mesomorphe β-Form von Polycapronamid und ihre Umwandlung in die kristalline Form α. Kolloid-Zeitschrift 167 (1959) 132–141.
- [28] D. Cavallo, L. Gardella, G.C. Alfonso, G. Portale, L. Balzano, R. Androsch, Effect of cooling rate on the crystal/mesophase polymorphism of polyamide 6, Colloid Polym. Sci. 289 (2011) 1073–1079.
- [29] R. Aelion, Preparation and structure of some new types of polyamides, Annali di Chimica Applicata 3 (1948) 5–61.
- [30] L.J. Mathias, D.G. Powell, J.P. Autran, R.S. Porter, ¹⁵N NMR characterization of multiple crystal forms and phase transitions in polyundecanamide (Nylon 11), Macromolecules 23 (1990) 963–967.
- [31] D. Mileva, R. Androsch, E. Zhuravlev, C. Schick, Morphology of mesophase and crystals of polyamide 6 prepared in a fast scanning chip calorimeter, Polymer 53 (2012) 3994–4001.
- [32] D. Mileva, I. Kolesov, R. Androsch, Morphology of cold-ordered polyamide 6, Colloid Polym. Sci. 290 (2012) 971–978.
- [33] A. Mollova, R. Androsch, D. Mileva, C. Schick, A. Benhamida, Effect of supercooling on crystallization of polyamide 11, Macromolecules 46 (2013) 828–835.
- [34] R. Androsch, C. Schick, Crystal nucleation of polymers at high supercooling of the melt, Adv. Polym. Sci. 276 (2017) 257–288.
- [35] A. Toda, R. Androsch, C. Schick, Insights into polymer crystallization and melting by fast scanning chip calorimetry, Polymer 91 (2016) 239–263.
- [36] C. Schick, R. Androsch, J.W.P. Schmelzer, Homogeneous crystal nucleation in polymers, J. Phys. Condens. Matter (2017) (submitted 2017).
- [37] A.M. Rhoades, R. Androsch, I. Stolte, C. Schick, Density of heterogeneous and homogeneous crystal nuclei in poly (butylene terephthalate), Eur. Polym. J. 66 (2015) 180–189.
- [38] A.M. Rhoades, N. Wonderling, A. Gohn, J. Williams, D. Mileva, M. Gahleitner, R. Androsch, Effect of cooling rate on crystal polymorphism in beta-nucleated isotactic polypropylene as revealed by a combined WAXS/FSC analysis, Polymer 90 (2016) 67–75.
- [39] A.M. Rhoades, N. Wonderling, C. Schick, R. Androsch, Supercooling-controlled heterogeneous and homogenous crystal nucleation of polyamide 11 and its effect onto the crystal/mesophase polymorphism, Polymer 106 (2016) 29–34.
- [40] H.W. Starkweather, R.E. Brooks, Effect of spherulites on the mechanical properties of nylon 66, J. Appl. Polym. Sci. 1 (1959) 236–239.
- [41] L. Shen, I.Y. Phang, T. Liu, Nanoindentation studies on polymorphism of nylon 6, Polym. Test. 25 (2006) 249–253.
- [42] Zytel Molding Guide, 25 1 2017. [Online]. Available: http://www2. dupont.com/ Plastics/en_US/assets/downloads/processing/198118E.pdf, accessed 15.05.17.
- [44] A.M. Rhoades, J.L. Williams, R. Androsch, Crystallization kinetics of polyamide 66 at processing-relevant cooling conditions and high supercooling, Thermochim. Acta

- 603 (2015) 103-109.
- [45] H. Haberkorn, K.H. Illers, P. Simak, Molekülordnung und Kristallinität in Polyhexamethylenadipamid, Colloid Polym. Sci. 257 (1959) 820–840.
- [46] M. Hirami, SAXD studies on bulk crystallization of nylon 6. I. Changes in crystal structure, heat of fusion, and surface free energy of lamellar crystals with crystallization temperature, J. Macromol. Sci. Phys. B 23 (1984) 397–414.
- [47] Q. Zia, R. Androsch, H.-J. Radusch, S. Piccarolo, Morphology, reorganization and stability of mesomorphic nanocrystals in isotactic polypropylene, Polymer 47
- (2006) 8163-8172.
- [48] D. Mileva, R. Androsch, H.-J. Radusch, Effect of structure on light transmission in isotactic polypropylene and random propylene-1-butene copolymers, Polym. Bull. 62 (2009) 561–571.
- [49] Q. Zia, R. Androsch, H.-J. Radusch, Effect of the structure at the micrometer and nanometer scale on the light transmission of isotactic polypropylene, J. Appl. Polym. Sci. 117 (2010) 1013–1020.